Monthly Notices
of the
ROYAL ASTRONOMICAL SOCIETY

Mon. Not. R. Astron. Soc. **407,** 969–985 (2010) doi:10.1111/j.1365-2966.2010.16990.x

A census of nuclear stellar discs in early-type galaxies

H. R. Ledo,[1⋆] M. Sarzi,[1] M. Dotti,[2] S. Khochfar[3] and L. Morelli[4]

[1]*Centre for Astrophysics Research, University of Hertfordshire, College Lane, Hatfield AL10 9AB*
[2]*Max-Planck-Institut für Astrophysik, Karl-Schwarzschild-Str. 1, D-85748 Garching, Germany*
[3]*Max-Planck-Institute für extraterrestrische Physik, Giessenbachstraβe, D-85748 Garching, Germany*
[4]*Dipartimento di Astronomia, Università di Padova, vicolo dell Osservatorio 2, 35122 Padova, Italy*

Accepted 2010 May 8. Received 2010 April 19; in original form 2010 February 17

ABSTRACT

Nuclear stellar discs (NSDs), of a few tens to hundreds of parsec across, are a common and yet poorly studied feature of early-type galaxies. Still, such small discs represent a powerful tool to constrain the assembling history of galaxies, since they can be used to trace to the epoch when galaxies experienced their last major merger event. By studying the fraction and stellar age of NSDs, it is thus possible to test the predictions for the assembly history of early-type galaxies according to the current hierarchical paradigm for galaxy formation. In this paper we have produced the most comprehensive census of NSDs in nearby early-type galaxies by searching for such discs in objects within 100 Mpc and by using archival images from the *Hubble Space Telescope*. We found that NSDs are present in approximately 20 per cent of early-type galaxies, and that the fraction of galaxies with NSDs depends neither on their Hubble type nor on their galactic environment, whereas the incidence of NSDs appears to decline in the most massive systems. Furthermore, we have separated the light contribution of 12 such discs from that of their surrounding stellar bulge in order to extract their physical properties. This doubles the number of decomposed NSDs and although the derived values for their central surface brightness and scalelength are consistent with previous studies, they also give a hint of possible different characteristics due to different formation scenario between nuclear discs and other kinds of large galactic discs.

Key words: galaxies: bulges – galaxies: elliptical and lenticular, cD – galaxies: evolution – galaxies: formation.

1 INTRODUCTION

More than a decade ago, *Hubble Space Telescope* (*HST*) observations revealed the presence of nuclear stellar discs in several galaxies (van den Bosch et al. 1994). These discs are distinct nuclear components with a few tens to hundreds of parsecs in diameter and have since then been recognized as a relatively common feature in early-type galaxies (e.g. Rest et al. 2001) while being notably rare in spirals (Pizzella et al. 2002). Despite the relatively high frequency of NSDs, only a few studies were aimed at deriving their fundamental properties (Scorza & van den Bosch 1998; Pizzella et al. 2002; Morelli et al. 2004; Balcells et al. 2007), whereas the interest in NSD revolved mainly around their dynamically cold character, which facilitates the mass measurement of central supermassive black holes (SMBHs) (e.g. van den Bosch & de Zeeuw 1996).

Yet, NSDs may constitute a unique tool to constrain the assembling history of galaxies. NSDs are indeed fragile structures that should not survive a major merger event involving their host galaxy, which makes them useful clocks to trace the epoch since such an event occurred. Simple *N*-body simulations serve to illustrate the delicate nature of NSDs (Fig. 1). Following Dotti et al. (2007) we set up a stable stellar disc that is 200 pc across, 10^8 $M_\odot$ in mass and which is orbiting around a central SMBH of the same mass in the total gravitational potential dictated also by the stellar bulge and dark-matter halo. We have then let loose a second 10^8 $M_\odot$ SMBH 80 pc above the galactic plane in a nearly circular polar orbit and follow the evolution of the disc. Given that early-type galaxies share the same black-hole mass content (Ferrarese & Merritt 2000; Gebhardt et al. 2000), the interaction with a second SMBH of the same mass serves to explore in conservative way (without even considering the interaction with the stars around the second SMBH) the impact on the disc of a merging event with second galaxy of similar mass. Fig. 1 shows how after just 2.5 Myr the interaction with the alien SMBH has considerably disrupted the structure of the disc, which by becoming more vertically extended and radially concentrated would be very hard to detect.

A systematic study of the incidence of NSD in early-type galaxies could therefore help in constraining their assembling history, which, contrary to their star formation history (e.g. Thomas et al. 2005), is poorly understood. According to the standard hierarchical paradigm for galaxy formation, the most massive galaxies should

⋆E-mail: h.ledo@herts.ac.uk

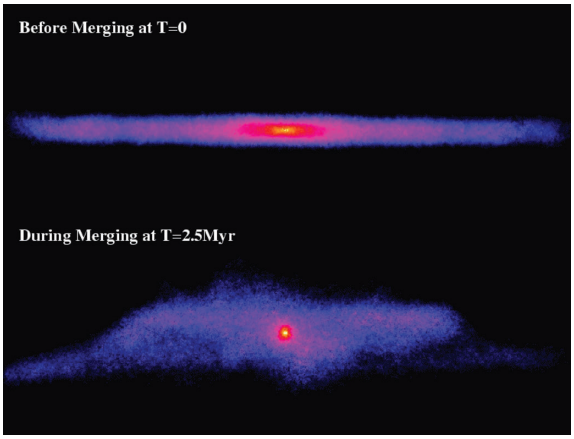

Figure 1. *N*-body simulation illustrating the fragility of nuclear stellar discs during major merger events. The top panel shows a stable nuclear disc 200 pc in diameter and 10^8 $M_\odot$ in mass that is orbiting an SMBH of the same mass in the total gravitational potential dictated also by the bulge and the dark matter particles, which are not shown for the sake of clarity. A second 10^8 $M_\odot$ SMBH is let loose in a nearly circular polar orbit 80 pc above the galactic plane, to simulate the impact with a second galaxy of similar mass. The lower panel illustrates the disruption suffered by the disc after just 2.5 Myr, which would be even greater if the bulge and dark matter particle from the incoming galaxy would have been included in the simulation.

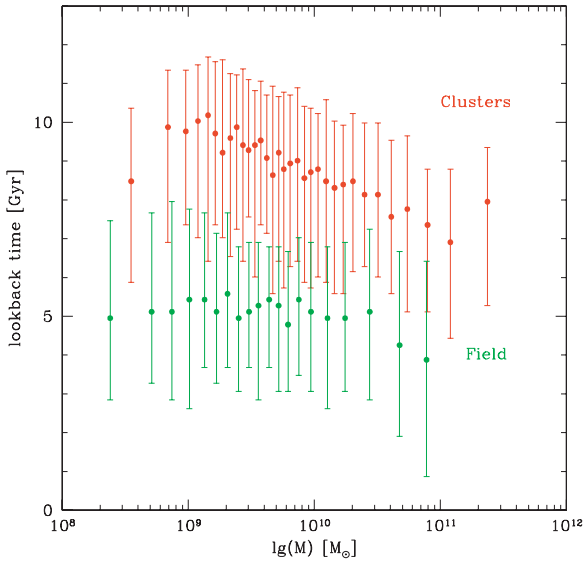

Figure 2. Prediction of semi-analytical models from Khochfar & Silk (2006a,b) for the age of the last major merger event experienced by galaxies of different masses and in different environments. Field early-type galaxies appear to have assembled later than those in clusters. In clusters, the models also predict a clear dependence on mass, with larger galaxies assembling later.

have been the last to reach their final configuration as they follow the merging paths of their host dark-matter haloes. The galactic environment should also play a role since once galaxies enter very crowded environments such as galaxy clusters, it is more difficult for them to merge due to the high relative velocities with which they cross each other. These dependencies are illustrated in Fig. 2, which shows the predictions of the semi-analytical models of Khochfar & Silk (2006a,b) for the epoch of the last major merger experienced by galaxies of different masses and living in cluster or field environments. Semi-analytical models can also track whether the last merging events involved considerable amount of gas as well as the probability that a small gas-rich companion was subsequently acquired, which will then determine whether an NSD is found today. Numerical simulations (e.g. Barnes & Hernquist 1996; Mayer et al. 2007; Hopkins & Quataert 2010) have indeed shown that when gas is involved in a merger event, it is always driven towards the centre of the remnant where it could then form a disc, depending on its angular momentum. Such a scenario has been invoked to explain the dichotomy seen in elliptical galaxies (e.g. Khochfar & Burkert 2005; Kormendy et al. 2009). NSDs could also provide constraints on the assembling history of their host galaxies in a more direct way, by dating the disc stellar population. In general, we expect the age of the stellar disc to represent a lower limit to the look-back time since the epoch of the last major merger event experienced by their host galaxy, since the NSD could have formed also after such an event, unless the last major merger was a gas-rich event that led also to the formation of nuclear disc itself.

As a first step to use NSDs as tools to constrain the assembling history of early-type galaxies, in this paper we will provide for the first time a complete census of the nearby NSD population, providing also estimates for basic physical properties such as their mass and extent. This work will provide the basis for further investigations which will assess the fragility of the NSD identified here using a more comprehensive set of numerical simulations. Such set of fragile discs will constitute a sample for spectroscopic follow-up aimed at deriving their stellar ages, while the incidence of such fragile discs could be compared with the prediction of semi-analytical models.

This paper is organized as follows. To compile such a census we had to define a sample and retrieve the images (Section 2), to look for discs in these galaxies and to separate the discs from the bulges in order to find their properties (Section 3). The results will be presented in Section 4 and the conclusions in Section 5.

2 SAMPLE SELECTION AND DATA MINING

2.1 Selection and acquisition

For this study we have selected, using the LEDA data base (Paturel et al. 2003), all early-type galaxies (*E*, *E*-*S*0, *S*0 and *S*0*a*) within 100 Mpc so as to produce a volume-limited sample. This list was then cross-correlated with the *HST* archive and all the galaxies with images from the WFPC2 and ACS cameras were requested, preferably the filters F555W and F606W. In some cases these filters were not available and others had to be chosen. The use of different passbands should not bias our estimates of the disc inclination and extent; however, as shown by Morelli et al. (2010), nuclear discs do not present strong radial colour gradients.

After downloading the available images they were checked for their quality and those saturated, too dusty or in which the galaxy was lying at the edge of the detector were discarded since in these cases it would have been impossible to find NSDs even if they were present. In the end we collected a sample of 466 early-type galaxies with *HST* images, out of a parent LEDA sample of 6801 galaxies.

2.2 Sample properties

Having a sample, we retrieved the global parameters of our galaxies. Of particular interest are M_B and an estimate of the galactic environment, because they directly relate to the general questions we are trying to answer, and the galaxy inclination because it influences our ability to find the discs. The magnitude of our galaxies

and an estimate for their inclination values are available from the LEDA data base whereas to obtain a value for the galactic density we used the Nearby Galaxies Catalogue of Tully (1988).

Although the distribution of M_B and environment values for our *HST* sample and its parent LEDA sample are somewhat different, this does not pose as a problem when we are dealing with the incidence of NSD. Indeed in this case it only matters that in each magnitude bin we have enough objects to obtain secure estimates for the NSD fraction. Also, inclination differences do not matter for constraining the incidence of NSDs, as long as the distribution of inclination in each *HST* subsample allows a reliable correction of the fraction of NSD (that is if there are enough galaxies where the disc could have been detected; see Section 4.1.1). On the other hand, we need to keep in mind that any conclusion on the structural properties of the NSDs, such as their typical size or mass, will be specific to our *HST* sample.

2.3 Inclination

The more face-on a disc is, the harder it is to identify it. Rix & White (1990) have studied this problem and concluded that for inclinations with $\cos(i) > 0.6$ it is impossible to detect discy signatures in the galaxy isophotes. The inclination, i, is defined as being 0° for face-on discs and 90° if they are edge-on.

Although we do not know for sure the inclination of the nuclear discs, we will assume that the vast majority of them will have the same inclinations of their host galaxies, which is justified if we consider our sample galaxies as oblate axisymmetric spheroids. The LEDA data base provides inclination estimates for the host galaxies based on the method applied by Heidmann, Heidmann & de Vaucouleurs (1972) and Bottinelli et al. (1983). The inclination was calculated assuming that all galaxies of a given Hubble type had an axis ratio equal to that observed in the flattest galaxy of that type. By construction, this method provides a conservative lower estimate for our galaxies' inclination, since intrinsically rounder galaxies in a given Hubble type would in reality have a higher inclination. Using such lower estimates to correct the fraction of NSD will lead to an upper limit on their incidence, whereas the uncorrected fraction provides a lower limit as if we were assuming that all galaxies where edge-on.

3 ANALYSIS

3.1 Disc identification process

Having collected the *HST* images of 466 early-type galaxies, we systematically searched for the signature of the presence of an NSD, both in maps for the fine structure of the galaxy and in the shape of the galaxy isophotes.

We have used the code of Pogge & Martini (2002) to generate structure maps for each of our sample galaxies, taking care to use in each case the appropriate WFPC2 or ACS point-spread function from the TINY TIM code (Krist & Hook 2004).

We then fitted ellipses to the galaxy isophotes using the IRAF task *ellipse* and, in particular, extracted profiles for the galaxy ellipticity, ϵ, and the A_4 parameter which is the fourth coefficient of the cosine term of the Fourier expansion of the considered isophotes (Carter 1977; Jedrzejewski 1987). In practice, the A_4 parameter measures the deviation of the isophote's shape from a perfect ellipse, and is positive in the case of discy deviations.

The existence of a disc in our galaxies is often revealed by the structure maps, but to separate discs from otherwise simply highly flattened central regions (e.g. a flattened bulge or a larger galactic-scale disc), we seek for a distinct peak in both the ϵ and A_4 profiles.

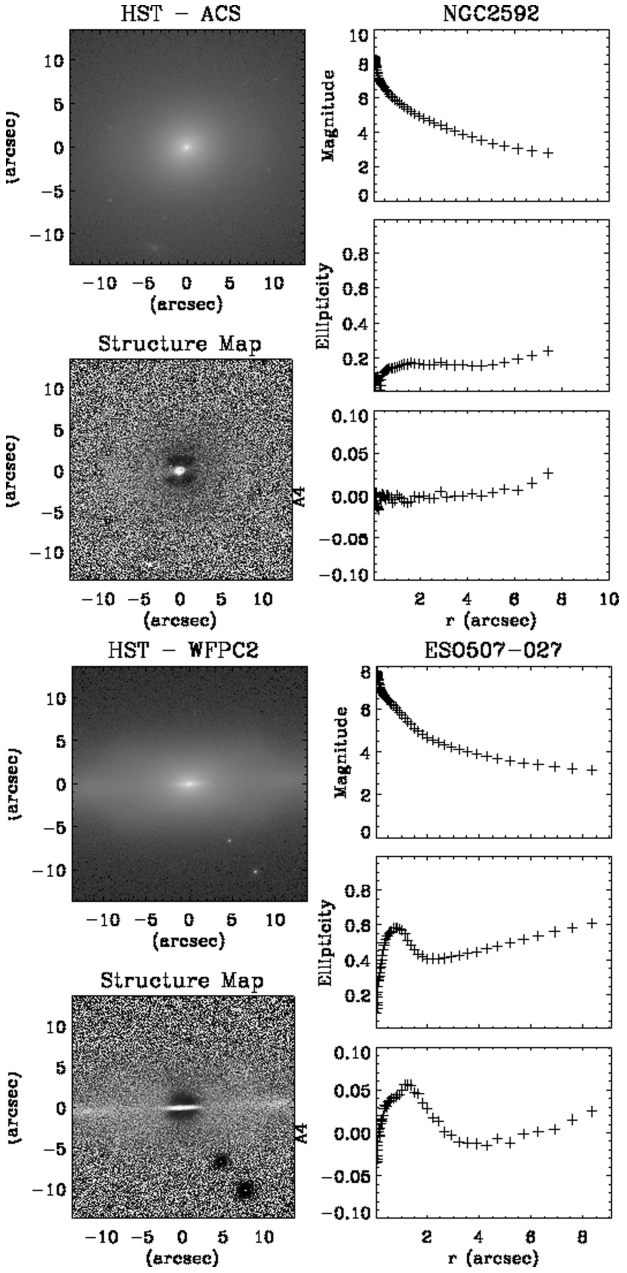

Figure 3. On the top panel we have the original image of NGC 2592, its structure map and magnitude, ellipticity and A_4 profiles where no nuclear stellar disc is visible and, on the bottom we have the same information for ESO507-027 where its presence is detected.

Fig. 3 illustrates our disc-identification procedure for two sample galaxies, one with and one without an NSD. Similar figures for all the galaxies where we identified the presence of a nuclear disc are presented in Appendix A.

3.2 Disc–bulge decomposition

Having identified which galaxies in our sample host an NSD, we now wish to investigate the basic properties of such discs by disentangling their contribution to the observed surface brightness distribution of the host galaxy. For early-type galaxies where the main

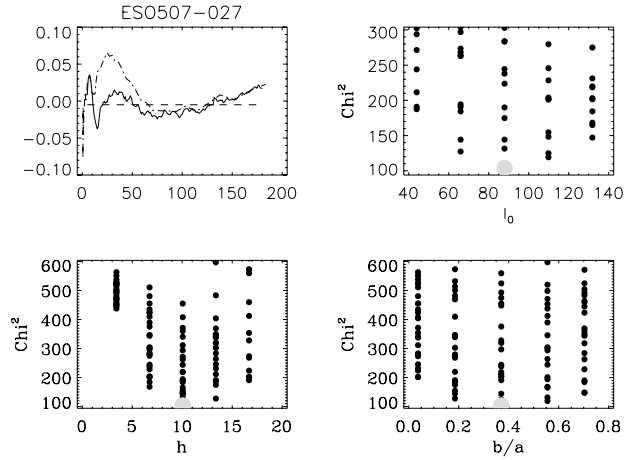

Figure 4. On the top left panel we can see A_4 profiles before (dot-dashed line) and after (solid line) Scorza and Bender decomposition for ESO507-027. The other three panels show the chosen parameters with their corresponding lower χ^2.

bulge component displays simple elliptical isophotes, we can adopt the algorithm devised by Scorza & Bender (1995), whereby the best disc parameters are sought by iteratively subtracting from the galaxy image an exponential disc model until the original signature of the disc is completely erased in the ϵ and A_4 profiles that are measured in the residual image. To perform the the Scorza and Bender decomposition on our sample nuclear discs we use the IDL implementation of this method of Morelli et al. (2004), where more details about the algorithm can be found.

Fig. 4 illustrates for the ESO507-027 how the discy deviations in the A_4 profile are minimized after the subtraction of the best exponential disc model. Appendix B shows similar figures for all NSD that were found embedded in an elliptical bulge, whereas Table A1 lists their basic parameters. In a few cases we report the values for the disc parameters from previous studies.

3.3 Disc size estimates

For a large fraction of the NSD that we identified we could not apply the previously described technique efficiently, mostly owing to the presence of dust or of an intrinsically boxy bulge, in particular if the boxiness changes with radius. Under these circumstances we can at least estimate the extent of the NSD by exploiting the fact that the position of the peak of the A_4 deviation introduced by the disc correlates loosely with the actual extent of the disc, as found in the objects for which a disc–bulge decomposition has been performed (Fig. 5). This allowed us to estimate the sizes of the discs which could not be decomposed with the Scorza and Bender method. They are listed in Table A2.

4 RESULTS

4.1 The census

By inspecting the structure maps and the isophotal shape of the central regions of 466 early-type galaxies, we have found evidence for a distinct disc component in 63 objects, corresponding to 13.52 per cent of our sample. Table 1 breaks down the observed fraction of NSDs as a function of galaxy type, whereas Tables 2 and 3 show the incidence of NSDs as a function of the *B*-band absolute magnitude and galactic environment, when such quantities could be measured.

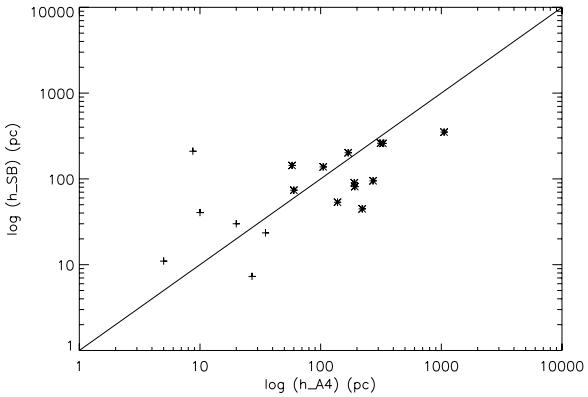

Figure 5. Relation between the sizes derived from the peak in the A_4 profile and those obtained from the Scorza and Bender decomposition. The asterisks represent the discs decomposed in this work and the crosses show discs decomposed in previous works (van den Bosch et al. 1994; Scorza & Bender 1995; Scorza & van den Bosch 1998; Morelli et al. 2004).

Table 1. As a function of galaxy Hubble type (column 1), the number of objects with *HST* images and of the NSDs found in them (columns 2 and 3) yield a lower limit on the incidence of NSDs in early-type galaxies (column 4). Using the fraction of objects where disc detection is possible (column 5), we can correct for inclination biases and obtain an upper limit on the fraction of NSDs (column 6).

Type (1)	*HST* (2)	NSDs (3)	$f_{\rm NSDs,obs}$ (4)	$f_{HST,\rm detect}$ (5)	$f_{\rm NSDs}$ (6)
E	219	22	10.04 ± 2.03	52.97	18.95 ± 4
E-S0	68	9	13.24 ± 4.11	63.24	20.9 ± 6.2
S0	109	21	19.27 ± 3.78	66.97	28.8 ± 5.3
S0-a	70	11	15.71 ± 4.35	64.29	24.44 ± 6.8
Total	466	63	13.52 ± 1.58	59.44	22.75 ± 2.52

Table 2. Same as Table 1 but as a function of the galaxy absolute *B*-band magnitude (column 1), which was not available for 14 objects.

$M_{\rm B}$ (1)	*HST* (2)	NSDs (3)	$f_{\rm NSDs,obs}$ (4)	$f_{HST,\rm detect}$ (5)	$f_{\rm NSDs}$ (6)
−24 to −22	16	0	0	81.3	0
−22 to −20	175	23	13.1 ± 2.6	59.4	22.1 ± 4.1
−20 to −18	174	34	19.5 ± 3.0	62.6	31.2 ± 4.4
−18 to −16	70	6	8.6 ± 3.4	51.4	16.7 ± 6.2
−16 to −15	17	0	0	53.0	0

4.1.1 Inclination correction and final values

As mentioned in Section 2.3, the inclination of the nuclear discs greatly affects our ability to detect them. It is indeed very likely that a considerable number of NSDs have escaped our detection because they lie in the equatorial plane of galaxies that are only slightly inclined from the plane of the sky, so that the NSDs appear close to face us. The fraction of NSDs deduced directly from the number of observed NSDs therefore represents only a lower limit for the true incidence of NSDs. We can estimate such true fraction considering that the number of NSDs that we have found should reflect the true fraction of NSD when considering only the systems

Table 3. Same as Table 1 but as a function of galactic environment (column 1), from Tully (1988). Only 191 objects were listed in this catalogue.

Density (1)	*HST* (2)	NSDs (3)	$f_{\rm NSDs,obs}$ (4)	$f_{HST,\rm detect}$ (5)	$f_{\rm NSDs}$ (6)
0-1	128	25	19.5 ± 3.5	19.5	33.3 ± 5.4
1-2	23	6	26.1 ± 9.2	26.1	35.3 ± 11.6
2-3	18	6	33.3 ± 11.1	33.3	42.9 ± 13.2
3-4	22	5	22.7 ± 8.9	22.7	41.7 ± 14.2

where NSDs could have in fact been detected, so that

$$f_{\rm NSD} = \frac{f_{\rm NSD,\,observed}}{f_{\rm detectable,\,NSD}}, \quad (1)$$

where $f_{\rm NSD,\,observed}$ is the observed fraction of NSDs in the entire sample and $f_{\rm detectable,\,NSD}$ is the fraction of galaxies where NSDs can be found. Using the estimates for the inclination of our sample galaxies that we retrieved in Section 2.3, we can compute $f_{\rm detectable,\,NSD}$ considering that according to Rix & White (1990) the ability to detect an embedded disc drops very quickly for $\cos(i) > 0.6$, independent of the relative disc contribution to the total light distribution. Using the previous equation, the fraction of galaxies with $\cos(i) < 0.6$ and considering that our inclination values are only lower estimates, we can correct our face values for the incidence of NSDs and obtain upper limits for such fractions. These are also listed in Tables 1, 2 and 3.

Table 1 indicates that approximately between 13 and 23 per cent of nearby early-type galaxies host nuclear stellar discs, without significant differences depending on their Hubble type. As regards the fraction of nuclear stellar disc as a function of their host absolute magnitude (Table 2), it would appear that the incidence of the discs peaks in the magnitude range between $M_{\rm B} = -20$ and -18, decreasing sharply in particular towards higher stellar luminosity where no NSD is found. In fact even accounting for the smaller number of surveyed systems in the -24 to -22 magnitude bin, we should have found 1–4 objects to be consistent with the fraction estimated in the -22 to -20 bin. Finally, there appears to be no significant trend with environment, at least as defined in Tully (1988), although we need to keep in mind that unfortunately only less than half of our sample was found in this particular catalogue.

4.2 Properties of the decomposed discs

We have applied the Scorza & Bender disc–bulge decomposition to 12 discs, which doubles the number of NSD that were previously analysed in this way. Although a few more NSDs appeared embedded in well-defined elliptical bulges, it was not possible to disentangle their light contribution. This is mainly because the observed A_4 profile does not appear to be well described by the simple model we used for the discs. Scorza & van den Bosch (1998) compiled all previous measurements for the structural properties of NSDs and plotted them together with other kinds of galactic discs in a μ_c^0–h plot which has later been updated by Morelli et al. (2004) and that we present in Fig. 6, to which we now add our own 12 objects. Although our values fall within the range found in previous results, confirming that NSDs follow a similar μ_c^0–h trend as that of embedded discs or main galactic discs, many of our decomposed NSDs appear to have a lower central surface brightness or smaller scale radius. In fact, the position of all NSDs in Fig. 6 suggests that these may follow a somewhat steeper and offset relation compared to bigger discs.

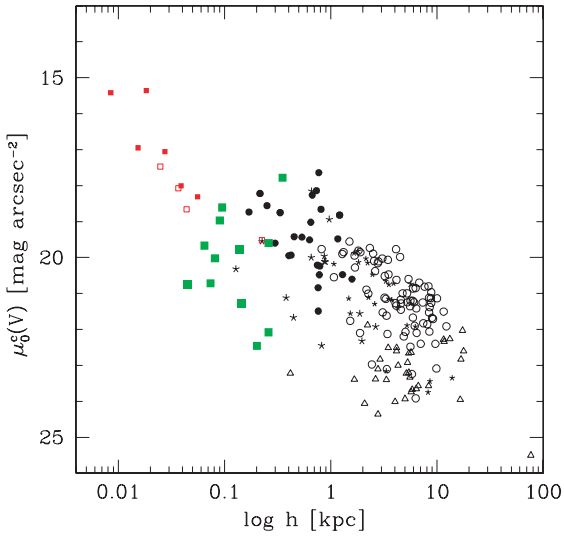

Figure 6. Discs' μ_0^c–h diagram from Morelli et al. (2004). The open circles correspond to high surface-brightness spiral galaxies whereas low surface-brightness spirals are represented by triangles. Stars denote S0s and filled circles discy ellipticals. NSDs in elliptical and lenticular galaxies are indicated by filled squares and in spirals by open squares. The larger green squares are those added in this work and the smaller red ones are the pre-existing ones.

5 CONCLUSIONS

Nuclear stellar discs have long been regarded as common features in early-type galaxies, but a quantitative assessment of such statements was still lacking prior to this work. By performing the most extensive volume-limited census of NSDs to date, we have now shown that between 13 and 23 per cent of nearby early-type galaxies host such systems. The incidence of nuclear stellar discs appears to decline in the most massive systems, consistent with the expectations that dry mergers dominated the most recent history of such objects (Khochfar & Burkert 2003; Khochfar & Silk 2009) and also with the finding that NSDs are exceedingly rare in brightest cluster galaxies (2 per cent, Laine et al. 2003). On the other hand, it is less clear what may cause the decrease in the fraction of NSDs that is found also at the faint end of our sample. Similarly, the lack of a dependence on galactic environment seems to contrast the first-order predictions of semi-analytical models (Fig. 2). In fact, according to these, galaxies in clusters should have assembled much earlier and thus there should have been more time to regrow a nuclear disc. On the other hand, galaxies in cluster may not have ample reservoirs of cold gas at their disposal, in particular if orbiting within the hot-gas halo of the cluster, so that the early assembly of clusters does not make the presence of nuclear discs in cluster galaxies much more likely than in their field counterparts.

Using the well-established technique of Scorza & Bender (1995) to disentangle the light contribution of embedded discs from that of their surrounding bulges, we have extracted the structural parameters of 12 out of the 63 NSDs that we have identified. By doubling the number of NSDs we have shown even more convincingly that NSDs, like other kinds of large galactic discs, follow a correlation between the central surface brightness μ_c^0 and scalelength h, although it would appear that NSDs obey a somewhat different relation with smaller scalelengths or fainter central surface brightness values. Considering that disc galaxies obey a very precise relation

between their total luminosity and their maximum rotation velocity (the Tully–Fisher relation, Tully & Fisher 1977) that may ultimately derive from the fact that they form in the dark matter haloes that surround and dominate the mass budget of galaxies (Steinmetz & Navarro 1999), it may not be completely unexpected that NSDs, by forming in the central and bulge-dominated regions of galaxies, may have different structural and dynamical properties than that of their larger relatives. In fact, it is also possible that the structural properties of NSDs vary when dealing with different kinds of early-type galaxies such as discy and boxy systems (Kormendy & Bender 1996). Although the main reason for failing to isolate the disc component in the presence of a bulge of varying boxiness with radius (Section 3.3) has mostly to do with an unclear a priori for the intrinsic A_4 profile that the bulge should have in the absence of a disc, we cannot exclude that in boxy ellipticals NSDs may have a different profile than exponential. Along the lines first suggested by Bender & Saglia (1999), NSDs in boxy ellipticals could be akin to the rapidly rotating components that in these objects are generally identified as kinematically decoupled cores, although in general such structure tend to extend over much larger scales than NSDs (McDermid et al. 2006), in particular for massive ellipticals with the oldest stellar populations.

Finally, although for the majority of the NSDs we could not clearly separate the disc and bulge contributions to the central light of their host galaxies, we have none the less estimated their sizes using as a reference radius the distance from the centre where the disciness of the central isophotes appears to peak. Such scalelength estimates, coupled with the μ_c^0–h relation that NSDs appear also to obey and the N-body simulations, will be used in future investigations to assess which of our sample NSDs are indeed fragile against major merging events, thus providing good targets for a spectroscopic follow up aimed at constraining their stellar ages and thus, the time of their last major merger.

ACKNOWLEDGMENTS

The authors would like to thank the referee Cecilia Scorza for her helpful comments. We acknowledge the use of the HyperLeda database (http://leda.univ-lyon1.fr) NASA's Astrophysics Data System.

REFERENCES

Balcells M., Graham A. W., Peletier R. F., 2007, ApJ, 665, 1084
Barnes J. E., Hernquist L., 1996, ApJ, 471, 115
Bender R., Saglia R. P., 1999, in Merritt D. R., Valluri M., Sellwood J. A., eds, ASP Conf. Ser. Vol. 182, Galaxy Dynamics – A Rutgers Symposium. Astron. Soc. Pac., San Francisco, p. 113
Bottinelli L., Gouguenheim L., Paturel G., de Vaucouleurs G., 1983, A&A, 118, 4
Carter D., 1977, PhD thesis, Univ. Cambridge
Dotti M., Colpi M., Haardt F., Mayer L., 2007, MNRAS, 379, 956
Ferrarese L., Merritt D., 2000, ApJ, 539, L9
Fouqué P., Solanes J. M., Sanchis T., Balkowski C., 2001, A&A, 375, 770
Gebhardt K. et al., 2000, ApJ, 539, L13
Heidmann J., Heidmann N., de Vaucouleurs G., 1972, MNRAS, 75, 85
Hopkins P. F., Quataert E., 2010, MNRAS, 405, L41
Jedrzejewski R. I., 1987, MNRAS, 226, 747
Khochfar S., Burkert A., 2003, ApJ, 597, L117
Khochfar S., Burkert A., 2005, MNRAS, 359, 1379
Khochfar S., Silk J., 2006a, ApJ, 648, L21
Khochfar S., Silk J., 2006b, MNRAS, 370, 902
Khochfar S., Silk J., 2009, MNRAS, 397, 506
Kormendy J., Bender R., 1996, ApJ, 464, L119
Kormendy J., Fisher D. B., Cornell M. E., Bender R., 2009, ApJS, 182, 216
Krist C., Hook R., 2004, Tiny Tim User's Guide
Laine S., van der Marel R. P., Lauer T. R., Postman M., O'Dea C. P., Owen F. N., 2003, AJ, 125, 478
McDermid R. M. et al., 2006, MNRAS, 373, 906
Mayer L., Kazantzidis S., Madau P., Colpi M., Quinn T., Wadsley J., 2007, Sci, 316, 1874
Morelli L. et al., 2004, MNRAS, 354, 753
Morelli L., Cesetti M., Corsini E. M., Pizzella A., Dalla Bontà E., Sarzi M., Bertola F., 2010, A&A, in press (arXiv:1004.2190)
Paturel G., Petit C., Prugniel P., Theureau G., Rousseau J., Brouty M., Dubois P., Cambrésy L., 2003, A&A, 412, 45
Pizzella A., Corsini E. M., Morelli L., Sarzi M., Scarlata C., Stiavelli M., Bertola F., 2002, ApJ, 573, 131
Pogge R. W., Martini P., 2002, ApJ, 569, 624
Rest A., van den Bosch F. C., Jaffe W., Tran H., Tsvetanov Z., Ford H. C., Davies J., Schafer J., 2001, AJ, 121, 2431
Rix H.-W., White S. D. M., 1990, ApJ, 362, 52
Scorza C., Bender R., 1995, A&A, 293, 20
Scorza C., van den Bosch F. C., 1998, MNRAS, 300, 469
Steinmetz M., Navarro J. F., 1999, ApJ, 513, 555
Thomas D., Maraston C., Bender R., Mendes de Oliveira C., 2005, ApJ, 621, 673
Tully R. B., 1988, Nearby Galaxies Catalog. Cambridge Univ. Press, Cambridge
Tully R. B., Fisher J. R., 1977, A&A, 54, 661
van den Bosch F. C., de Zeeuw P. T., 1996, MNRAS, 283, 381
van den Bosch F. C., Ferrarese L., Jaffe W., Ford H. C., O'Connell R. W., 1994, AJ, 108, 1579

APPENDIX A: NUCLEAR STELLAR DISCS

A1 Properties of the galaxies with discs

Table A1. Properties of the decomposed discs where h is the scalelength, the inclination is as defined in Section 2.3 and $\mu^c_{0,V}$ is the central surface brightness.

Galaxy name	h (pc)	Inclination (°)	$\mu^c_{0,V}$ (mag arcsec^{-2})
ESO352-057	$44.74 \pm ^{23.16}_{16.05}$	$76.26 \pm ^{8.58}_{22.42}$	$20.74 \pm ^{1.05}_{1.04}$
ESO378-020	$53.39 \pm ^{33.51}_{18.54}$	$65.98 \pm ^{16.78}_{19.69}$	$19.1 \pm ^{1.27}_{0.58}$
ESO507-027	$94.87 \pm ^{23.22}_{16.8}$	$68.28 \pm ^{7.83}_{9.61}$	$18.61 \pm ^{0.47}_{0.37}$
IC0875	$259.67 \pm ^{59.41}_{77.71}$	$84.84 \pm ^{2.29}_{2.31}$	$22.08 \pm ^{0.63}_{0.4}$
NGC 0584	$90.18 \pm ^{24.82}_{18.37}$	$73.86 \pm ^{6.93}_{4.96}$	$18.97 \pm ^{0.6}_{0.28}$
NGC 3385	$351.19 \pm ^{52.33}_{55.07}$	$61.71 \pm ^{1.55}_{5.08}$	$17.78 \pm ^{0.06}_{0.16}$
NGC 3610	$260.38 \pm ^{44.81}_{79.84}$	$81.81 \pm ^{4.19}_{1.6}$	$19.60 \pm ^{0.77}_{0.2}$
NGC 4128	$138.01 \pm ^{43.84}_{38.68}$	$85.76 \pm ^{1.95}_{0.92}$	$19.77 \pm ^{0.67}_{0.21}$
NGC 4474	$143.5 \pm ^{59.28}_{59.21}$	$86.49 \pm ^{2.36}_{2.23}$	$21.29 \pm ^{1.21}_{0.54}$
NGC 4621	$73.87 \pm ^{13.71}_{24.26}$	$83.97 \pm ^{2.59}_{2.02}$	$20.72 \pm ^{0.6}_{0.32}$
NGC 4660	$81.19 \pm ^{12.32}_{27.19}$	$78.92 \pm ^{4.19}_{3.99}$	$20.02 \pm ^{0.51}_{0.33}$
NGC 5308[a]	$201.59 \pm ^{30.21}_{45.56}$	$89.89 \pm ^{-}_{-}$	$22.46 \pm ^{-}_{-}$

[a]We were unable to derive the errors for the inclination.

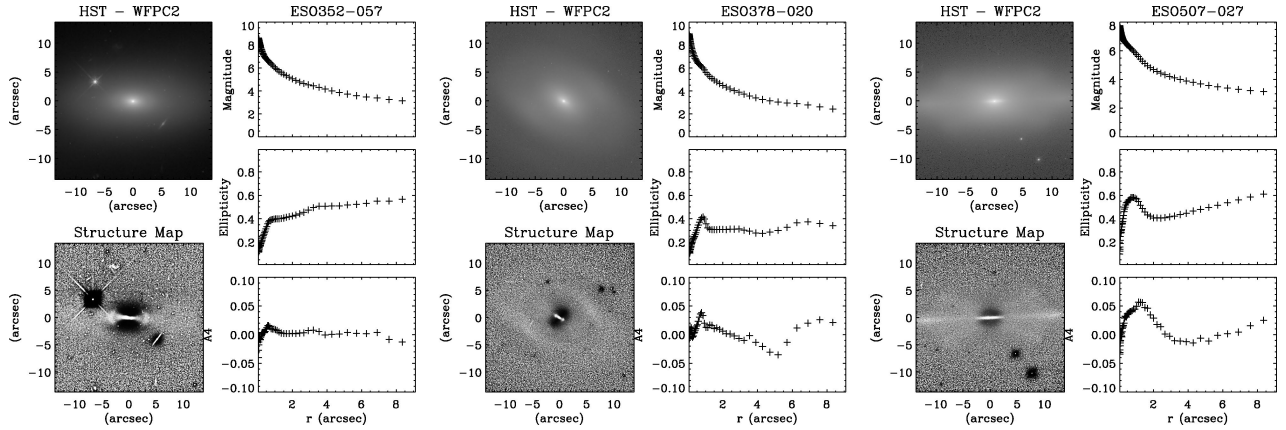

Figure A1. ESO352-057 on the left panel, in the middle ESO378-020 and ESO507-027 at the right. The original images and the structure maps are shown on the left of each panel and on the right we can see the surface brightness, ellipticity and A_4 profiles.

A2 NSD structure maps, ellipticity and A_4 profiles

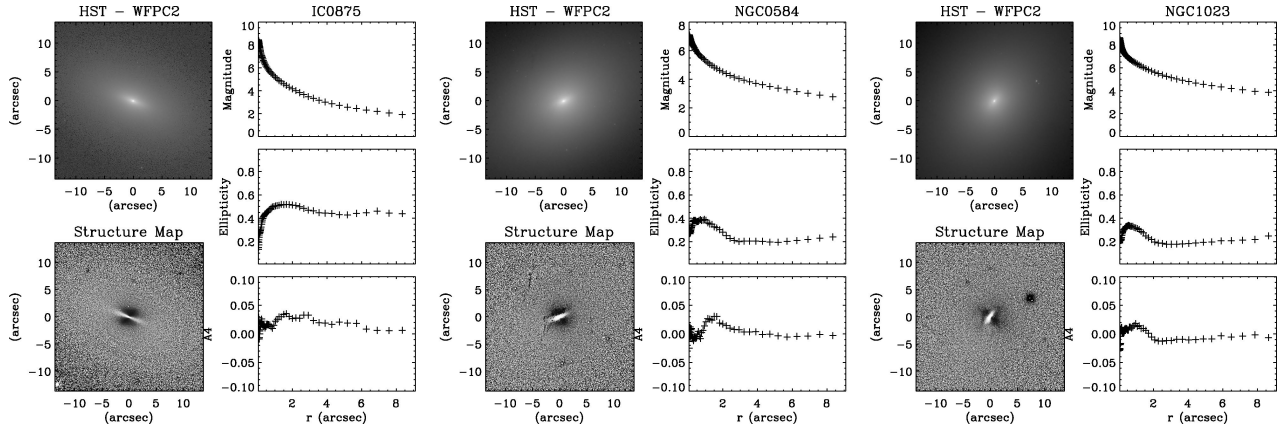

Figure A2. IC0875 on the left, NGC 0584 in the middle and NGC 1023 on the right.

Table A2. Galaxies where discs were found and some of their properties; (1) Galaxy's name; (2) Hubble type; (3) $\log_{10}$ of the axis ratio; (4) $\log_{10}$ of the apparent major axis diameter d25 at 25 mag arcsec^{-2}; (5) Disc inclination; (6) Absolute *B*-magnitude; (7) Radial velocity corrected for Local Group infall towards Virgo (208 km s^{-1}); (8) Distance derived from (7) and assuming $H_0 = 72$ km s^{-1} Mpc^{-1}, except for Virgo cluster members for which we adopted a common distance of 18 Mpc (Fouqué et al. 2001); (9) Density from Tully (1988); (10) Disc size with the indication in (11) of the source of the values, where *M* are those measured with the decomposition procedure, *E* have been estimated using the peak of the A_4 and *L* come from the literature.

Name	Type	logr_{25}	logd_{25}	Inclination (°)	$m_{\rm abs}$	*V*_Vir (km s^{-1})	Distance (Mpc)	Density (Mpc^{-3})	Disc size (pc)	Source
(1)	(2)	(3)	(4)	(5)	(6)	(7)	(8)	(9)	(10)	(11)
ESO352-057	S0	0.327	1.014	82.98	−19.842	5736.2	76.11	–	44.74	M
ESO378-020	S0	0.243	1.186	68.17	−19.899	5479.7	39.87	–	53.39	M
ESO507-027	S0	0.682	1.251	90.0	−20.079	2870.7	43.27	–	94.87	M
IC0875	S0	0.234	1.16	67.23	−19.442	3115.4	42.32	–	259.67	M
NGC 0584	E	0.179	1.578	79.78	−20.891	3047.0	24.49	0.42	90.18	M
NGC 1023	E-S0	0.377	1.868	76.7	−20.914	769.9	10.69	0.57	57	E
NGC 1129	E	0.42	1.444	90.0	−21.604	5404.8	75.07	–	146	E
NGC 1351	E-S0	0.189	1.532	65.35	−19.004	1301.0	18.07	1.57	131	E
NGC 1381	S0	0.421	1.405	90.0	−19.338	1520.6	21.12	1.54	131	E
NGC 1426	E	0.175	1.457	78.27	−19.092	1263.2	17.54	0.66	43	E
NGC 1427	E	0.179	1.636	71.35	−19.399	1159.2	16.10	1.59	16	E
NGC 1439	E	0.02	1.473	23.03	−19.507	1486.8	20.65	0.45	130	E
NGC 2549	S0	0.594	1.563	90.0	−19.445	1248.6	17.34	0.13	42	E
NGC 2685	S0-a	0.272	1.636	68.79	−19.092	1094.2	15.2	0.13	66	E

Table A2 – *continued*

Name	Type	$\log r_{25}$	$\log d_{25}$	Inclination (°)	m_{abs}	V_vir (km s^{-1})	Distance (Mpc)	Density (Mpc^{-3})	Disc size (pc)	Source
(1)	(2)	(3)	(4)	(5)	(6)	(7)	(8)	(9)	(10)	(11)
NGC 2787	S0-a	0.249	1.510	65.86	−19.645	949.0	13.18	0.06	115	E
NGC 2865	E	0.082	1.382	45.2	−20.792	2578.8	35.82	0.11	191	E
NGC 3115	E-S0	0.383	1.916	81.6	−20.042	642.6	8.93	0.08	30.0	L[a]
NGC 3156	S0	0.28	1.282	79.15	−18.512	1340.3	18.62	0.2	63	E
NGC 3377	E	0.327	1.588	90.0	−19.163	744.5	10.34	0.49	35	E
NGC 3384	E-S0	0.349	1.717	90.0	−19.826	917.1	12.74	0.54	49	E
NGC 3385	S0	0.267	1.182	72.56	−21.927	7824.4	108.67	–	351.19	M
NGC 3610	E	0.027	1.375	25.95	−20.664	1943.4	26.99	0.3	260.38	M
NGC 3613	E	0.315	1.544	90.0	−20.864	2232.9	31.01	–	15	E
NGC 3706	E-S0	0.167	1.477	61.64	−21.117	2817.9	39.14	0.27	114	E
NGC 3818	E	0.199	1.387	90.0	−19.389	1678.7	23.32	0.2	23	E
NGC 3900	S0-a	0.311	1.413	70.82	−20.168	1942.8	26.98	0.13	–	E
NGC 3945	S0-a	0.227	1.744	63.17	−20.085	1496.5	20.78	0.5	50	E
NGC 4026	S0	0.702	1.644	90.0	−19.592	1206.5	16.76	1.71	41	E
NGC 4128	S0	0.519	1.344	90.0	−20.041	2591.1	36.0	0.27	138.01	M
NGC 4270	S0	0.392	1.269	72.8	−19.702	2414.3	18.0	0.83	43.63	E
NGC 4318	E	0.167	0.869	79.12	−17.285	1297.6	18.02	1.47	70	E
NGC 4342	E-S0	0.297	1.101	90.0	−16.954	810.7	11.26	2.64	7.3	L[b]
NGC 4352	S0	0.331	1.231	90.0	−19.056	2164.4	18.0	–	17.45	E
NGC 4458	E	0.03	1.204	28.77	−17.437	770.0	10.69	3.21	11.0	L[c]
NGC 4473	E	0.235	1.630	90.0	−21.707	2338.1	18.0	2.17	183.26	E
NGC 4474	S0	0.174	1.368	57.3	−19.652	1707.6	18.0	3.8	143.5	M
NGC 4478	E	0.089	1.243	50.85	−19.602	1479.7	20.55	3.92	40.5	L[c]
NGC 4483	S0-a	0.282	1.265	71.34	−17.632	958.3	13.31	3.83	13	E
NGC 4515	E-S0	0.099	1.123	45.77	−17.775	1059.8	14.72	–	36	E
NGC 4528	S0	0.271	1.208	73.43	−18.874	1453.4	20.19	–	10	E
NGC 4546	E-S0	0.254	1.510	75.96	−19.726	1064.1	14.78	0.27	43	E
NGC 4570	S0	0.618	1.597	90.0	−20.444	1813.0	18.0	2.66	23.5	L[b]
NGC 4621	E	0.152	1.658	71.93	−20.789	527.1	18.0	2.6	73.87	M
NGC 4623	S0-a	0.477	1.352	90.0	−19.005	1863.7	18.0	2.36	210	L[d]
NGC 4660	E	0.124	1.323	61.24	−19.241	1185.1	18.0	3.37	81.19	M
NGC 4742	E	0.191	1.358	90.0	−19.376	1257.0	17.46	0.73	51	E
NGC 4762	S0	0.37	1.917	90.0	−19.921	1065.4	18.0	2.65	226.89	E
NGC 4866	S0-a	0.768	1.761	90.0	−20.727	2095.8	18.0	1.08	26.18	E
NGC 5076	S0-a	0.138	1.126	48.83	−19.491	2975.3	41.32	–	621	E
NGC 5252	S0	0.233	1.111	67.18	−21.039	6967.0	96.76	–	–	E
NGC 5308	S0	0.877	1.642	90.0	−20.439	2279.5	31.66	0.45	201.59	M
NGC 5838	E-S0	0.47	1.59	90.0	−20.05	1451	20.15	–	1684.2	L[e]
NGC 5854	S0-a	0.58	1.483	90.0	−19.698	1833.0	25.46	0.74	1147.9	L[e]
NGC 7173	E	0.088	1.275	47.16	−19.897	2368.8	32.90	0.35	48	E
NGC 7176	E	0.024	1.569	25.29	−20.423	2387.5	33.16	0.39	64	E
NGC 7562	E	0.137	1.338	67.29	−21.427	3571.8	49.61	–	–	E
NGC 7585	S0-a	0.123	1.406	46.52	−21.291	3432.0	47.67	–	69	E
NGC 7619	E	0.106	1.407	56.04	−21.987	3798.5	52.76	–	256	E
NGC 7785	E	0.283	1.447	90.0	−21.411	3875.7	53.83	–	497	E
PGC013343	E-S0	0.039	1.030	28.55	−16.909	1486.7	20.65	–	100	E
PGC036465	S0-a	0.307	0.825	67.59	−19.656	5736.2	79.67	–	232	E
PGC044815	S0	0.35	0.7	90.0	−18.58	6784	94.22	–	1005	E
UGC01003	S0	0.346	0.922	90.0	−19.488	5192.1	72.11	–	105	E
UGC03426	S0	0.096	1.224	42.78	−20.869	4292.5	59.62	–	58	E

[a]Scorza & Bender (1995).
[b]Scorza & van den Bosch (1998).
[c]Morelli et al. (2004).
[d]van den Bosch et al. (1994).
[e]Balcells et al. (2007).

A3 Disc decomposition

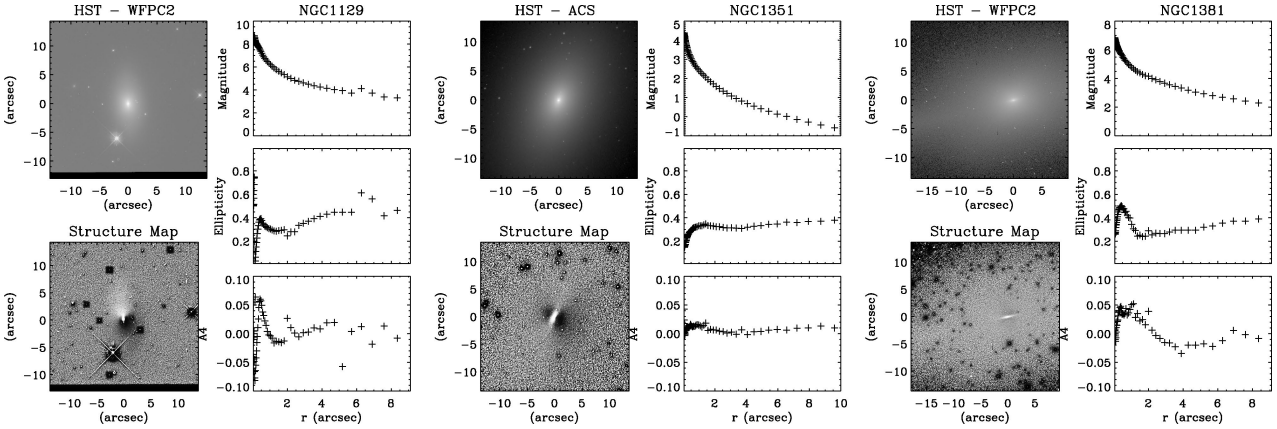

Figure A3. NGC 1129 on the left, NGC 1351 in the middle and NGC 1381 on the right.

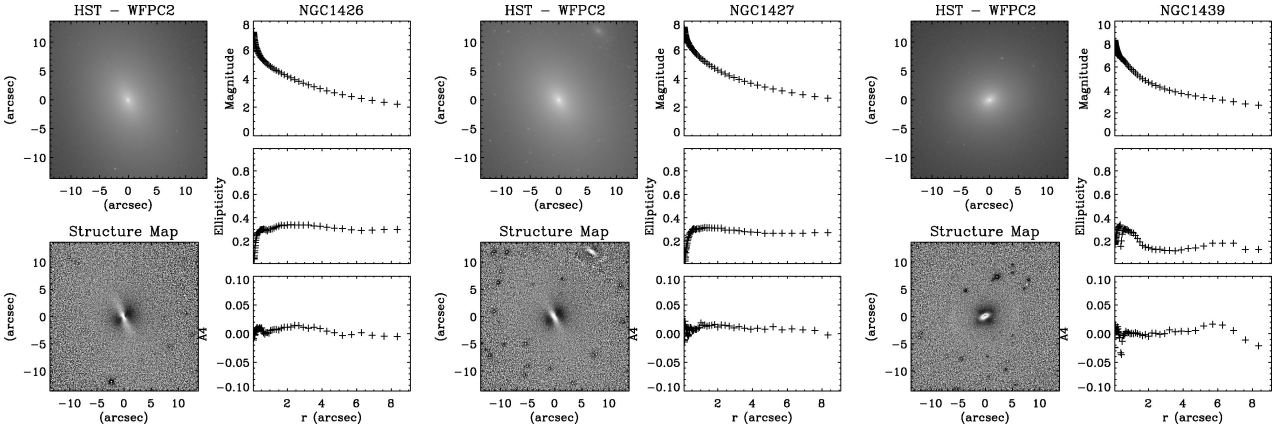

Figure A4. NGC 1426 on the left, NGC 1427 in the middle and NGC 1439 on the right.

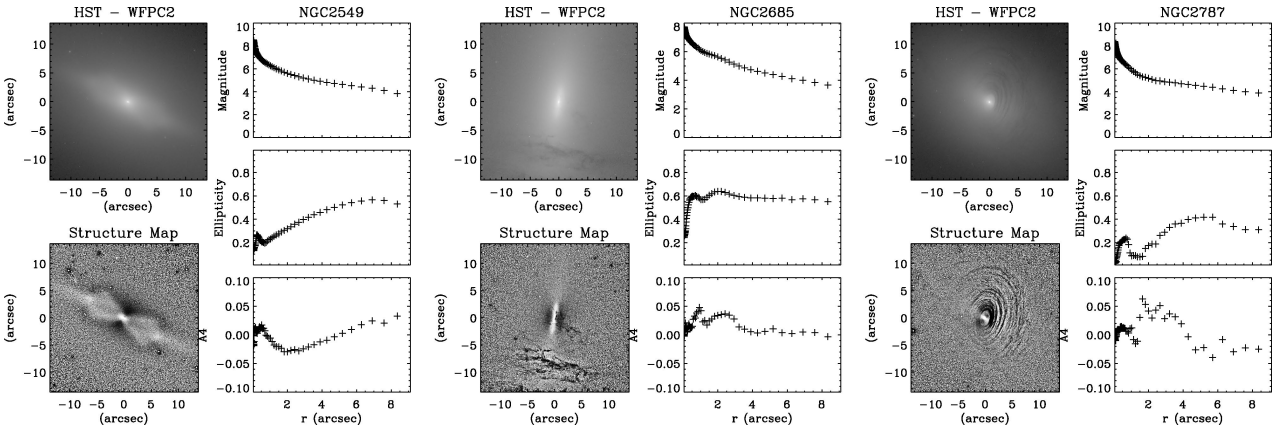

Figure A5. NGC 2549 on the left, NGC 2685 in the middle and NGC 2787 on the right.

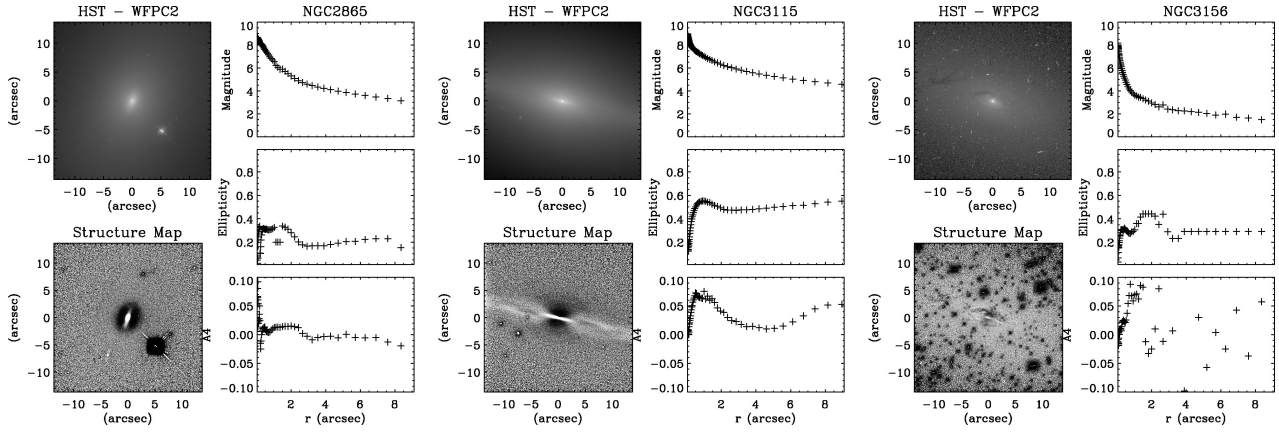

Figure A6. NGC 2865 on the left, NGC 3115 in the middle and NGC 3156 on the right.

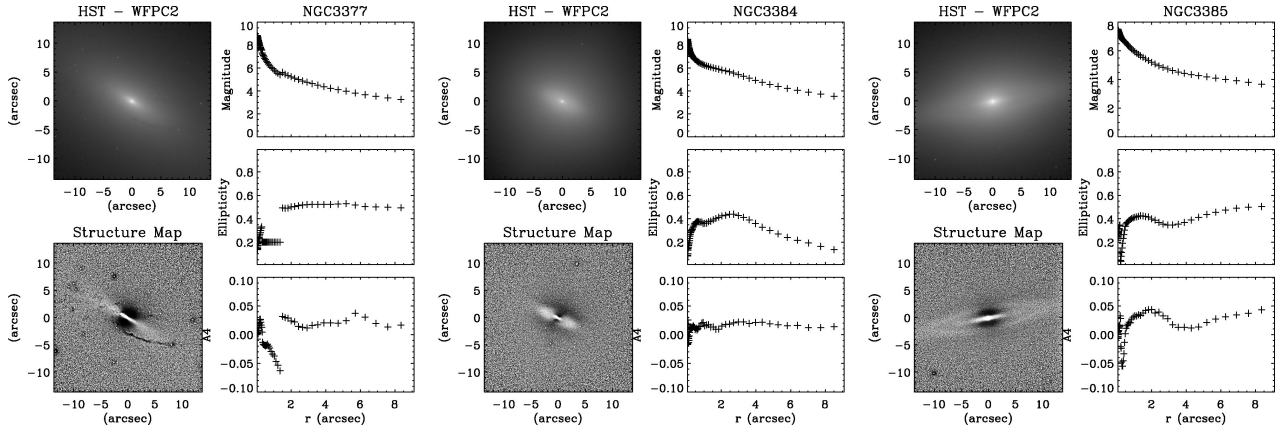

Figure A7. NGC 3377 on the left, NGC 3384 in the middle and NGC 3385 on the right.

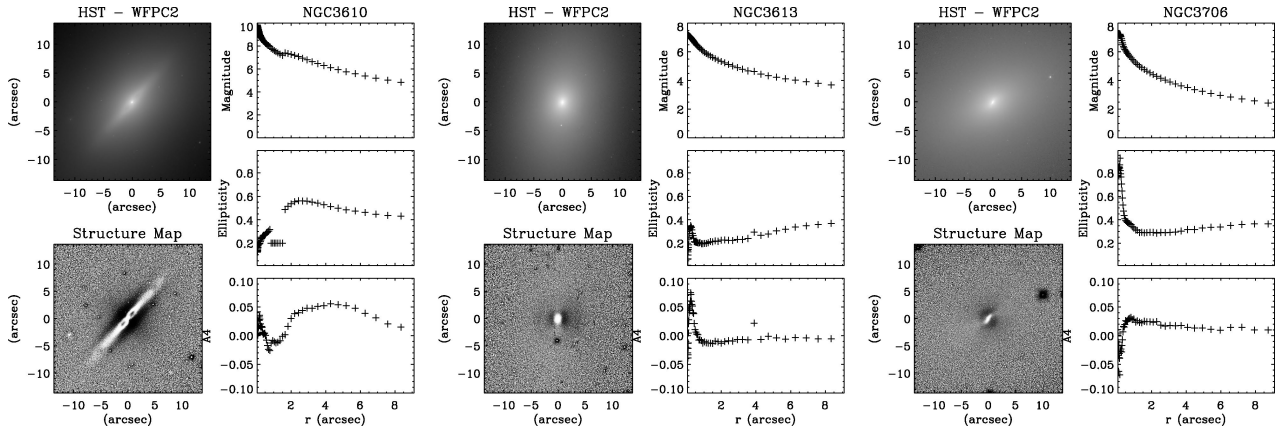

Figure A8. NGC 3610 on the left, NGC 3613 in the middle and NGC 3706 on the right.

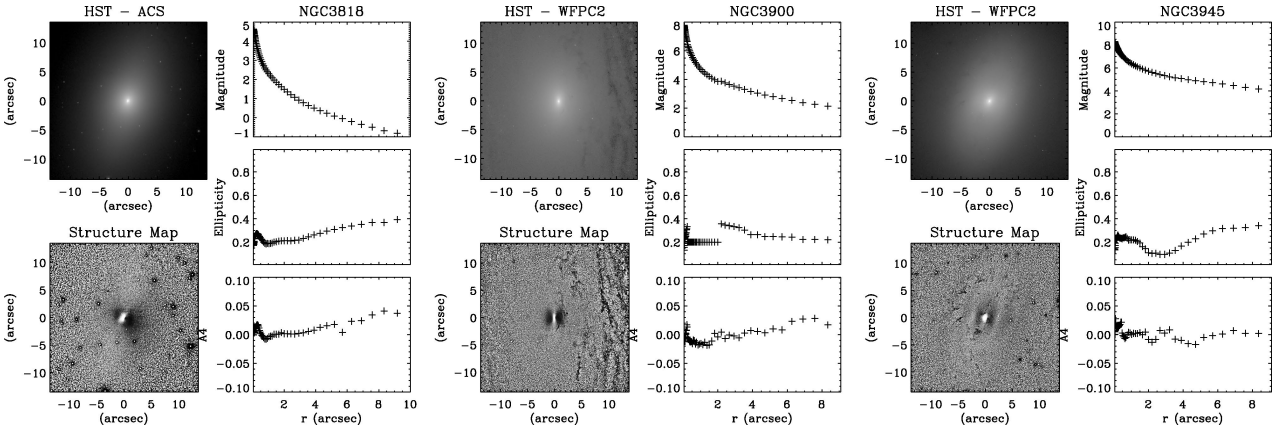

Figure A9. NGC 3818 on the left, NGC 3900 in the middle and NGC 3945 on the right.

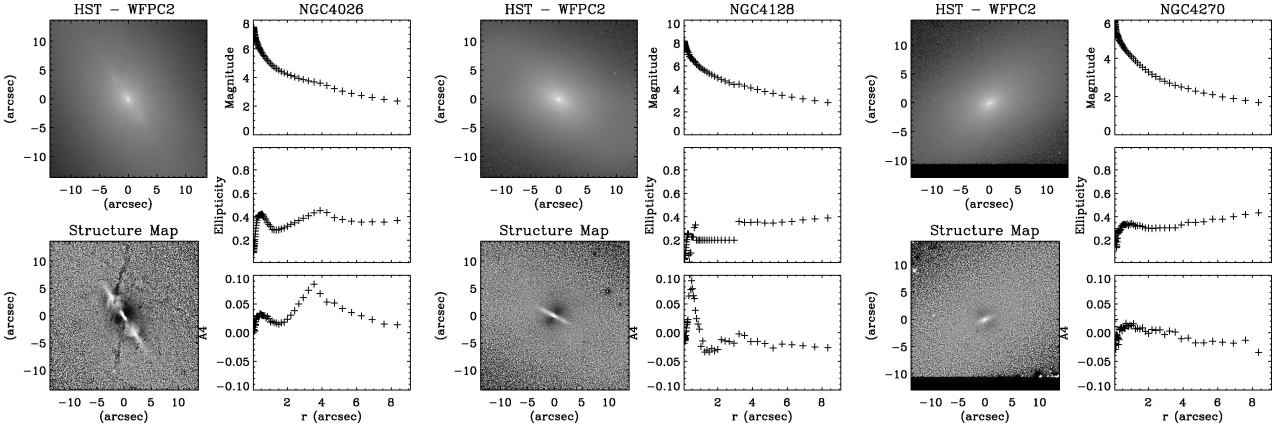

Figure A10. NGC 4026 on the left, NGC 4128 in the middle and NGC 4270 on the right.

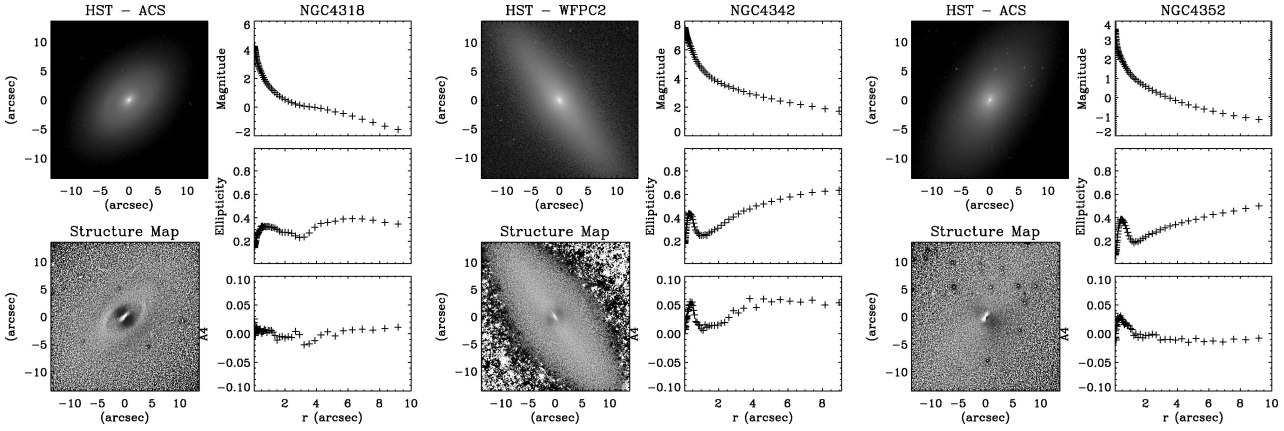

Figure A11. NGC 4318 on the left, NGC 4342 in the middle and NGC 4352 on the right.

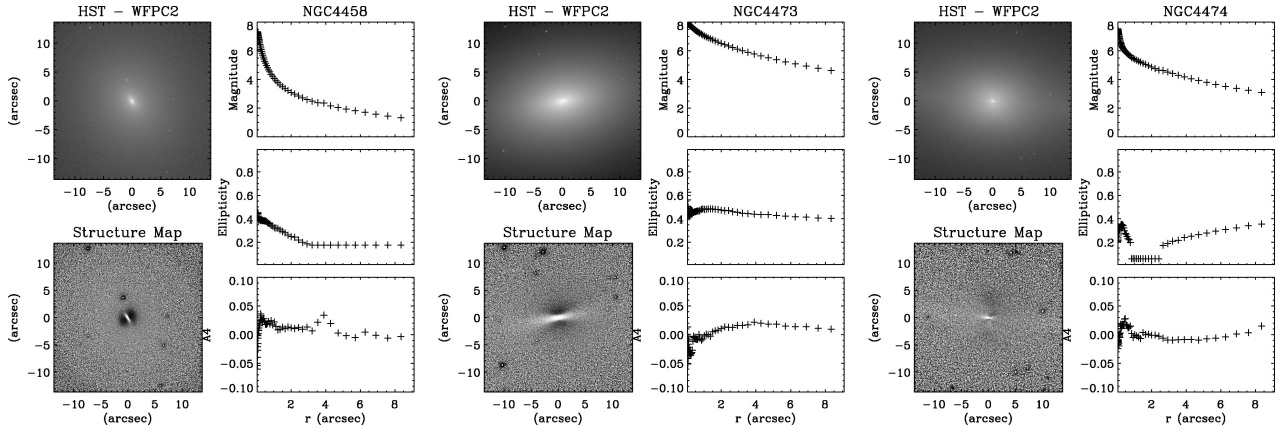

Figure A12. NGC 4458 on the left, NGC 4473 in the middle and NGC 4474 on the right.

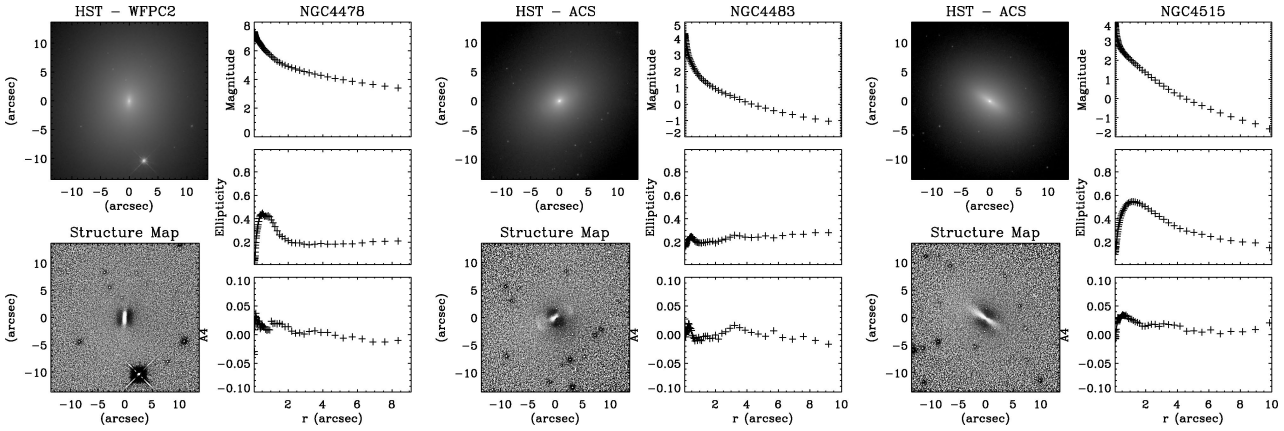

Figure A13. NGC 4478 on the left, NGC 4483 in the middle and NGC 4515 on the right.

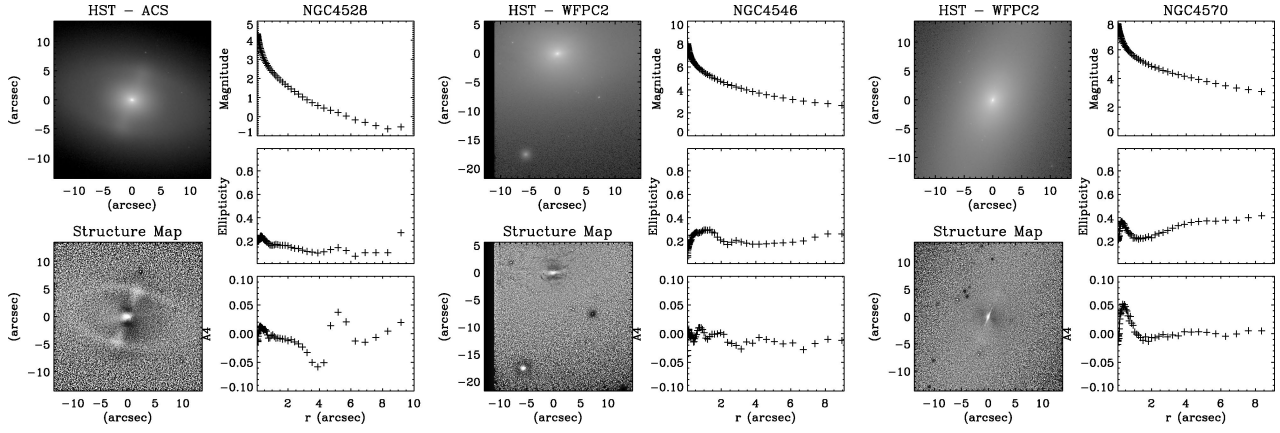

Figure A14. NGC 4528 on the left, NGC 4546 in the middle and NGC 4570 on the right.

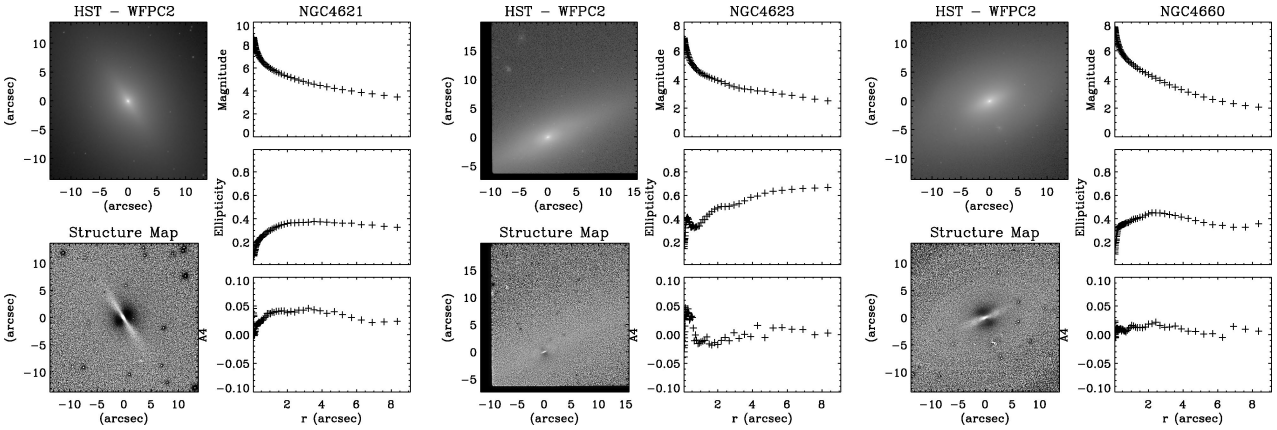

Figure A15. NGC 4621 on the left, NGC 4623 in the middle and NGC 4660 on the right.

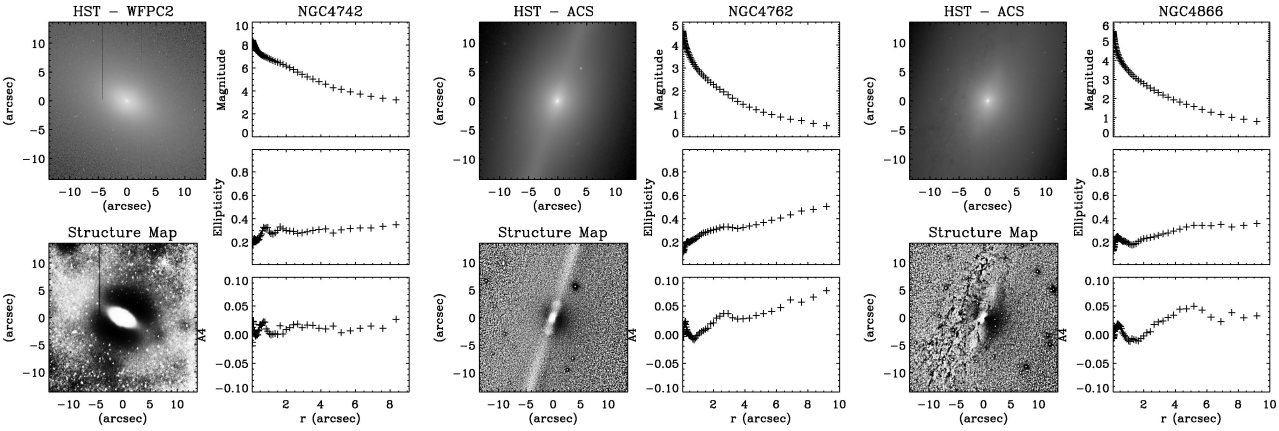

Figure A16. NGC 4742 on the left, NGC 4762 in the middle and NGC 4866 on the right.

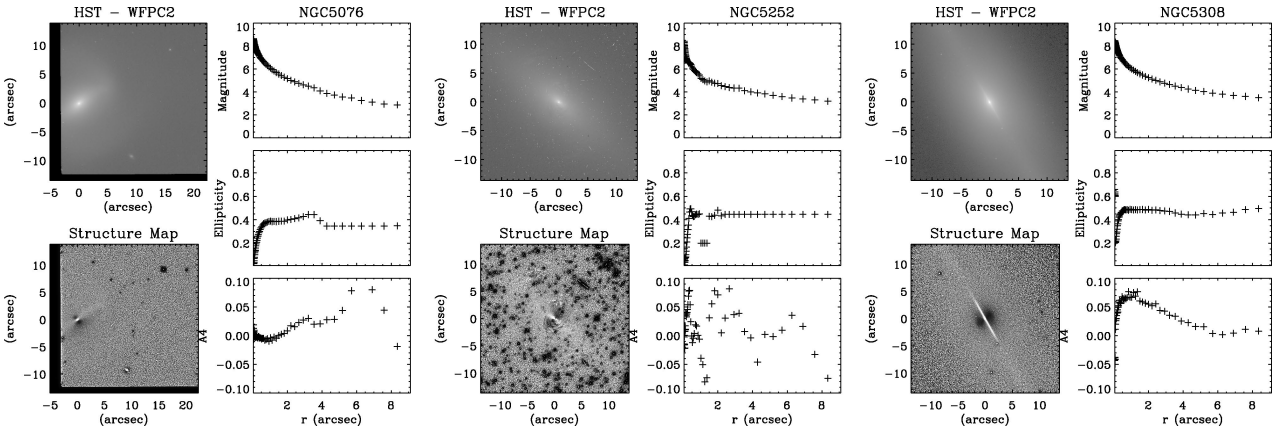

Figure A17. NGC 5076 on the left, NGC 5252 in the middle and NGC 5308 on the right.

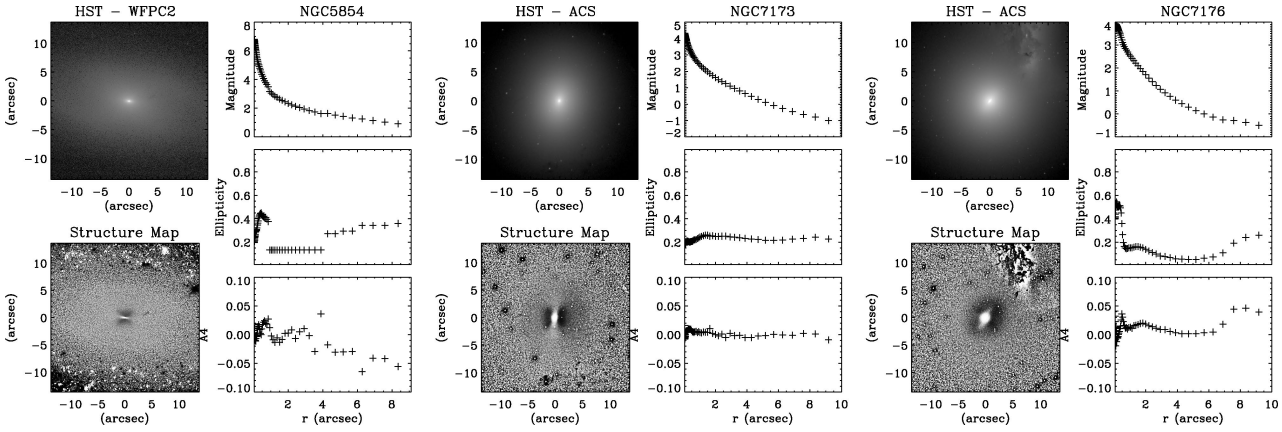

Figure A18. NGC 5854 on the left, NGC 7173 in the middle and NGC 7176 on the right.

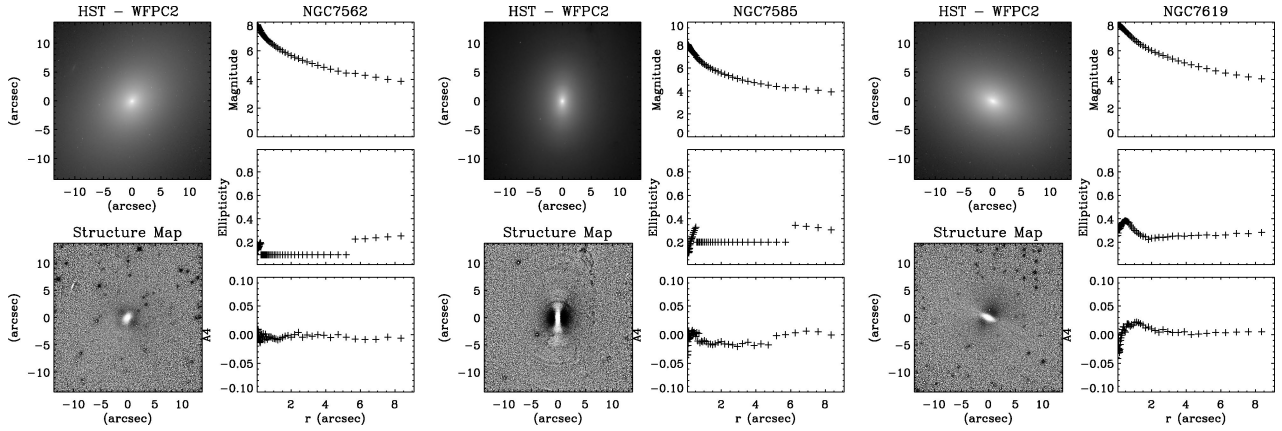

Figure A19. NGC 7562 on the left, NGC 7585 in the middle and NGC 7619 on the right.

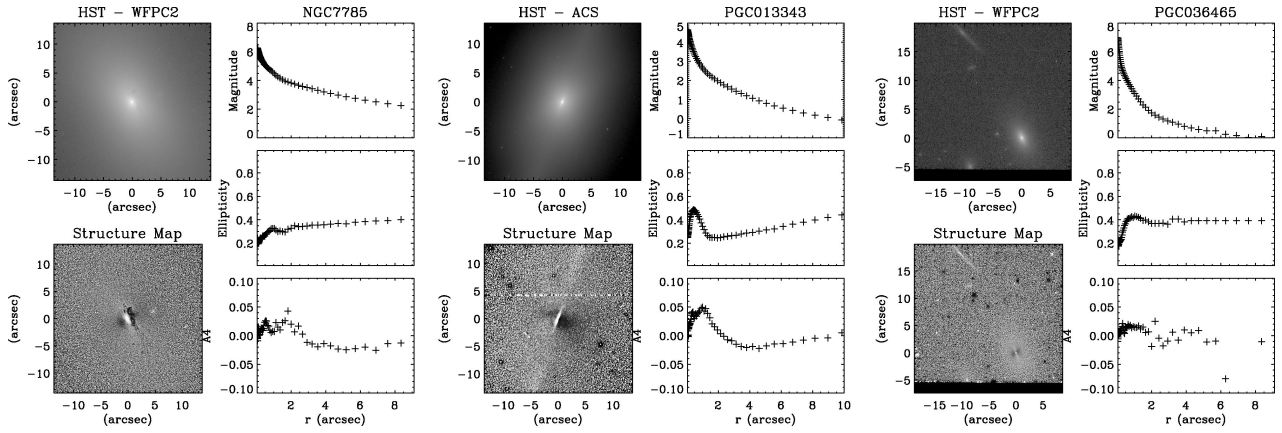

Figure A20. NGC 7785 on the left, PGC013343 in the middle and PGC036465 on the right.

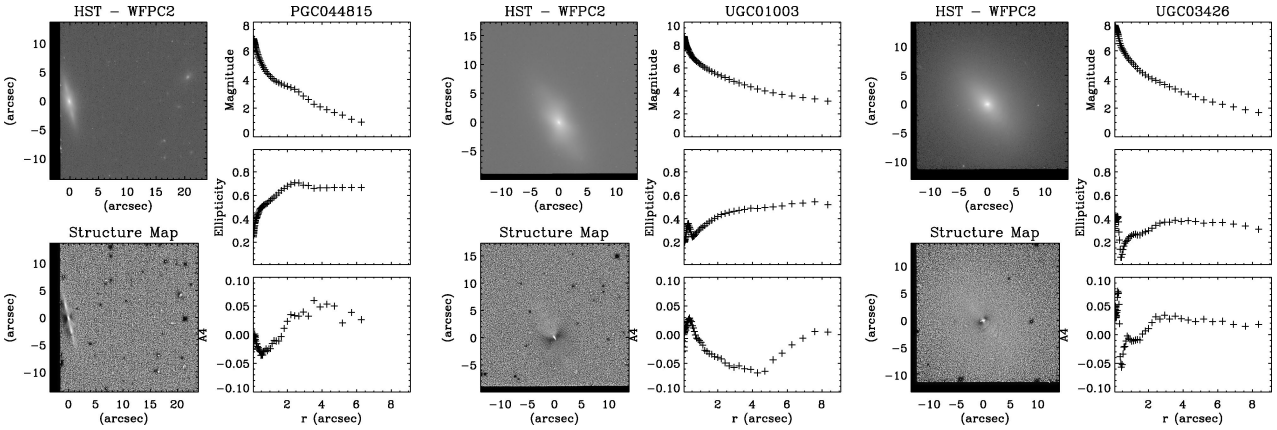

Figure A21. PGC044815 on the left, UGC01003 in the middle and UGC03426 on the right.

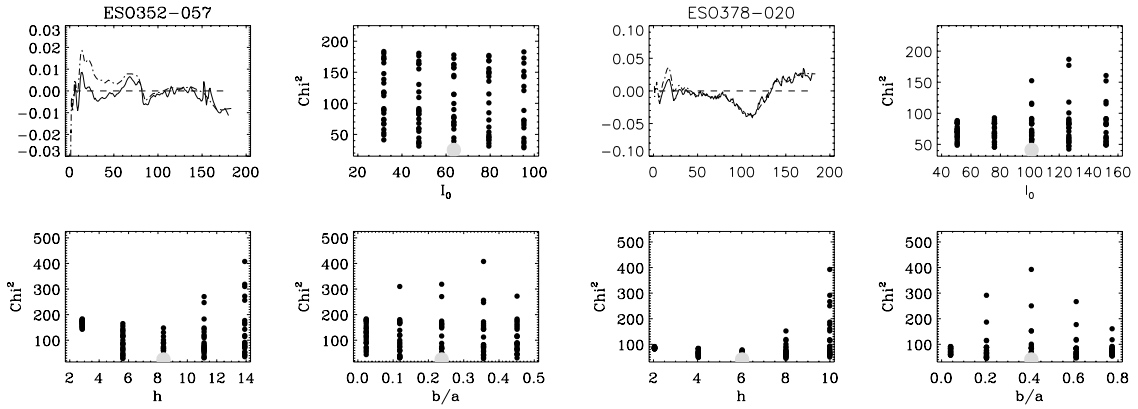

Figure A22. Scorza and Bender decomposition of ESO352-057 on the left and on the right.

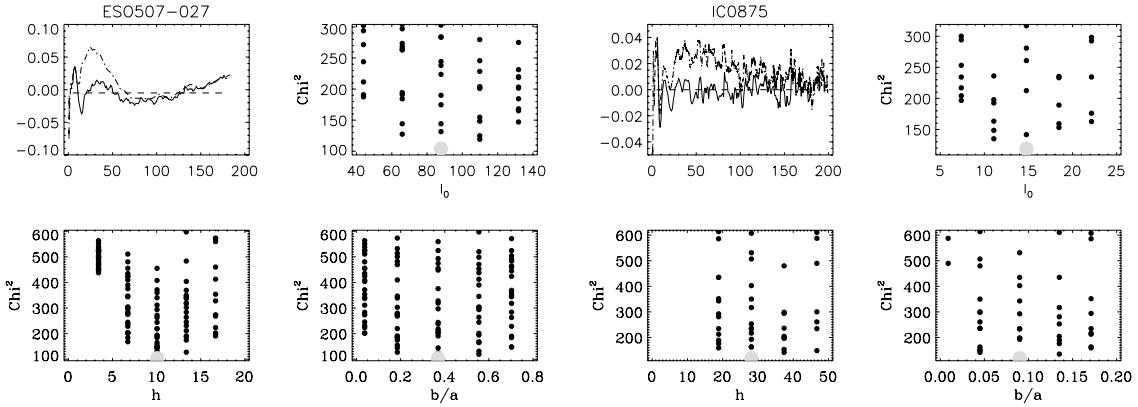

Figure A23. Scorza and Bender decomposition of ESO507-027 on the left and IC0875 on the right.

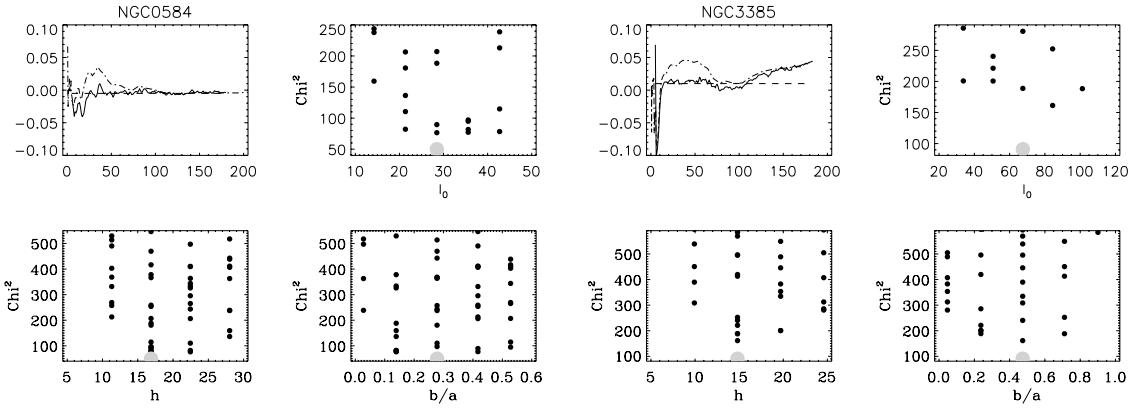

Figure A24. Scorza and Bender decomposition of NGC 0584 on the left and NGC 3385 on the right.

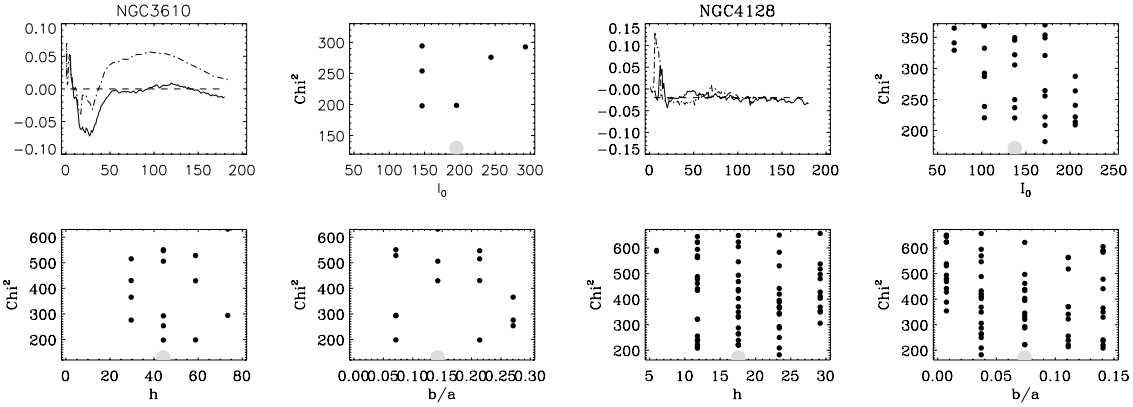

Figure A25. Scorza and Bender decomposition of NGC 3610 on the left and NGC 4128 on the right.

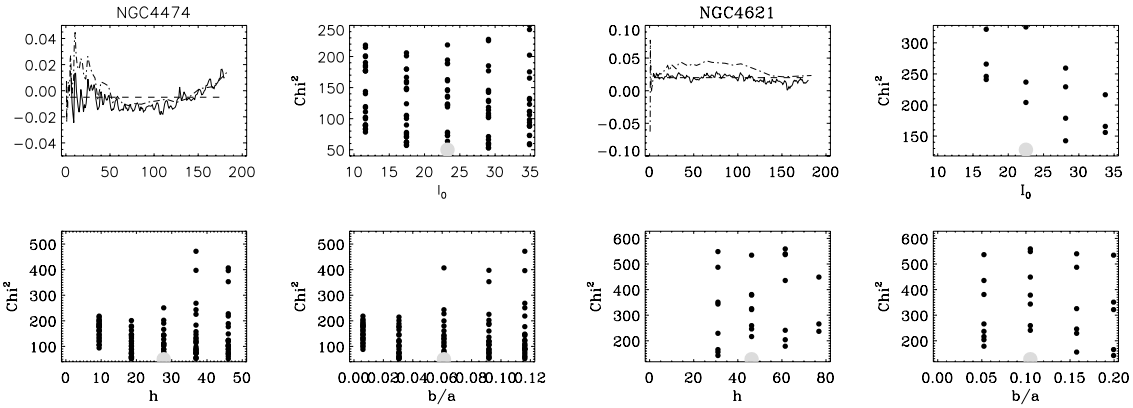

Figure A26. Scorza and Bender decomposition of NGC 4474 on the left and NGC 4621 on the right.

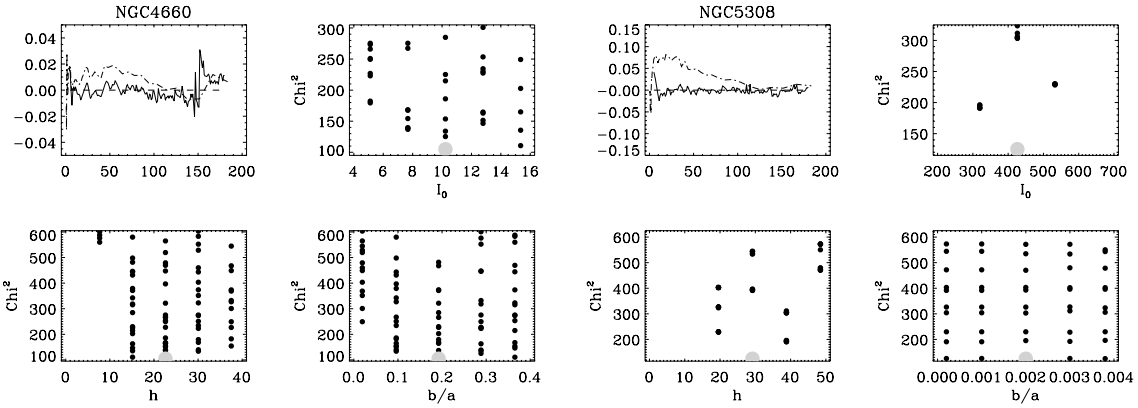

Figure A27. Scorza and Bender decomposition of NGC 4660 on the left and NGC 5308 on the right.

This paper has been typeset from a TEX/LATEX file prepared by the author.